



TECHNICAL NOTE

D-1272

AERODYNAMIC CHARACTERISTICS IN PITCH OF SEVERAL
RING-WING-BODY CONFIGURATIONS

AT A MACH NUMBER OF 2.2

By Odell Morris

Langley Research Center
Langley Station, Hampton, Va.

NATIONAL AERONAUTICS AND SPACE ADMINISTRATION
WASHINGTON

April 1962

NATIONAL AERONAUTICS AND SPACE ADMINISTRATION

TECHNICAL NOTE D-1272

AERODYNAMIC CHARACTERISTICS IN PITCH OF SEVERAL
RING-WING—BODY CONFIGURATIONS

AT A MACH NUMBER OF 2.2

By Odell Morris

SUMMARY

L
1
7
3
9

An investigation has been conducted in the Langley 4- by 4-foot supersonic pressure tunnel at a Mach number of 2.2 to determine the aerodynamic characteristics of several ring-wing—body configurations. This investigation included tests for the bodies alone and for the ring-wing—body combinations; these tests were conducted through an angle-of-attack range from about -4° to 11° .

The data indicated that sizable reductions in body wave drag were obtained for the concave-afterbody configuration as a result of the favorable interference produced by the ring wing. However, a large percentage of the total drag was produced by the ring wing and struts, and thus the ring-wing configurations of these tests appear to offer no drag advantage over a conventional wing-body configuration. Of the three configurations tested, the half-ring wing in combination with a body having a parabolic afterbody had the lowest drag (0.35) and the highest maximum lift-drag ratio (4.9).

INTRODUCTION

Considerable interest has been shown recently in ring-wing—body configurations as a means of reducing the wave drag. A number of theoretical studies has been made for this type of configuration and the results indicate that with proper wing-body design, a configuration with zero wave drag may be possible. (See refs. 1 to 3.) Results of the experimental investigations of references 4 to 6 on ring-wing configurations also provide data which show some drag reduction due to favorable interference effects.

However, in all of these investigations no overall measurements were made on the ring-wing—body configuration which included friction drag as well as wave drag. Reference 5 indicates that the magnitude of the friction drag from the large area of the ring wing may be sufficiently large to cancel the savings in wave drag. Thus, the overall configuration may not offer any drag advantage over a conventional wing-body configuration.

Accordingly, an experimental investigation has been conducted in the Langley 4- by 4-foot supersonic pressure tunnel to determine the aerodynamic characteristics in pitch of several ring-wing configurations at a Mach number of 2.2. These configurations were not specifically designed to produce zero wave drag but were tested primarily to measure the overall aerodynamic characteristics of a ring-wing—body combination and to show the possible wave-drag reduction for an arbitrary body shape of moderate fineness ratio. Tests were conducted for the body shapes alone and for the complete-ring-wing—body combinations through an angle-of-attack range from about -4° to 11° . The configurations investigated included a large-chord ring wing, a small-chord ring wing, and a small-chord half-ring wing in combination with bodies having three different afterbody shapes (cylindrical, parabolic, and concave). The results of the investigation, together with a limited analysis, are presented herein.

L
1
7
3
9

SYMBOLS

$C_{A,b}$	base axial-force coefficient, $\frac{(p_b - p)S_b}{qS_F}$
C_D	drag coefficient, $\frac{\text{Drag}}{qS_F}$
C_L	lift coefficient, $\frac{\text{Lift}}{qS_F}$
C_m	pitching-moment coefficient about wing quarter chord, $\frac{\text{Pitching moment}}{qS_F l}$
l	body length, in.
L/D	lift-drag ratio
M	free-stream Mach number

p	free-stream static pressure, lb/sq ft
p_b	body-base pressure, lb/sq ft
q	free-stream dynamic pressure, lb/sq ft
S_b	body-base area, sq ft
S_F	maximum body frontal area, 0.0123 sq ft
x,y	body coordinates, in.
α	angle of attack, deg

Subscript:

min minimum

Model components:

B_1	concave afterbody
B_2	parabolic afterbody
B_3	cylindrical afterbody
W_1	large ring wing (wing chord = 4.40 in.)
W_2	small ring wing (wing chord = 3.00 in.)
W_3	half-ring wing (wing chord = 3.00 in.)

MODEL AND APPARATUS

Details of the model configurations are illustrated in figure 1. Each of the three ring wings was a cylinder constructed of 0.075-inch-thick steel and was supported from the body by three mounting struts. Model wing components are designated by the letter W with subscripts 1, 2, and 3 to distinguish between the dimensional characteristics as indicated in figure 1(a). The body components are designated by the letter B with subscripts 1, 2, and 3 to distinguish between the afterbody shapes as shown in figure 1(b). Wing W_1 had the longest

chord (4.40 inches) and the largest planform area (21.6 square inches). Wing W_2 had a shorter chord (3.00 inches) and less planform area than wing W_1 , although the ring diameter was larger. Wing W_3 was a half-ring arrangement formed by removing the lower half of wing W_2 and repositioning the three mounting struts as shown in figure 1(a). The wings were placed on the body so that at a Mach number of 2.2 the leading edge of the ring wing would reflect the nose shock when at zero angle of attack. (See schlieren photographs of fig. 2.) The wings were composed of sections which had completely flat inner surfaces. The outer surface of each wing had a flat midsection with a wedge angle of 6° which tapered to a sharp edge at the wing leading and trailing edges.

The three bodies were constructed of steel and had an identical nose, parabolic in shape back to the 7.5-inch station. The three body shapes were formed by varying only the afterbody shapes (cylindrical, parabolic, and concave) as shown in figure 1(b). Coordinates for the different body shapes are given in table I.

The models were mounted in the tunnel on a remotely controlled sting. Forces and moments were measured by means of an internal strain-gage balance.

TESTS, CORRECTIONS, AND ACCURACY

The test conditions were as follows:

Mach number	2.2
Stagnation temperature, $^\circ\text{F}$	100
Stagnation pressure, lb/sq ft	1,150
Reynolds number per foot	1.8×10^6

The stagnation dewpoint was maintained sufficiently low (-25°F or less) to prevent condensation effects in the test section. The models were sting-mounted, and pitch tests of the bodies alone and of the complete models were made for an angle-of-attack range from about -4° to 11° . The angles of attack were corrected for deflection of the balance and sting under aerodynamic load. The pressure within the balance enclosure was measured, and the drag force was adjusted to correspond to a balance-chamber pressure equal to free-stream static pressure. A plot of the base axial-force coefficients against angle of attack is shown in figure 3. For most of the tests, except when noted in the figures, transition was fixed on the body and wing. Transition strips $1/8$ inch wide of No. 80 carborundum grains were applied along the

10-percent-chord line of the wing and at 10 percent of the body length rearward of the nose.

The accuracy of the measured quantities is estimated as follows:

C_D	±0.01
C_L	±0.05
C_m	±0.02
M	±0.01
α , deg	±0.1

PRESENTATION OF RESULTS

The results of the investigation and the figures in which they are presented are as follows:

Variation of body-base axial-force coefficient with angle of attack	3
Aerodynamic characteristics in pitch for isolated bodies	4
Aerodynamic characteristics in pitch for large ring wing in combination with three afterbodies	5
Drag breakdown for isolated bodies and for large ring wing and body combinations	6
Aerodynamic characteristics in pitch for the three ring-wing configurations with parabolic afterbody	7

SUMMARY OF RESULTS

The data of figures 4 and 5 show the aerodynamic characteristics in pitch for the isolated body configurations and for the large ring-wing-body combinations, respectively. All wing-body combinations show a stable pitching-moment slope with only negligible changes due to afterbody shape (fig. 5(a)); the variation of the lift coefficient with angle of attack was linear and essentially the same for each configuration. The differences in the drag coefficients and the lift-drag ratios among the complete configurations were very small (see fig 5(b)); however, the lowest minimum drag coefficient (0.528) and the highest L/D (4.1) were obtained for the ring-wing configuration with the concave afterbody (W_1B_1).

A drag breakdown for the isolated bodies and for the large ring wing and body combinations at zero angle of attack is presented in

figure 6. In order to evaluate the component drag, it was assumed that the ring wing W_1 in combination with the cylindrical afterbody B_3 would have no interference effects on body drag. Thus, the drag of the ring wing and struts was obtained by subtracting the isolated body drag of B_3 from the total wing-body drag of W_1B_3 . Body skin-friction estimates were made using Van Driest's skin-friction coefficients for turbulent flow. (See ref. 7.) For the bodies alone, the concave afterbody B_1 had the highest minimum total drag; however, for the ring-wing-bodies in combination, the configuration with the concave afterbody W_1B_1 had the lowest total drag. Comparison of the wave drag for the concave afterbody alone and with the wing indicates a reduction in the body wave drag of approximately 80 percent as a result of favorable interference. For the parabolic-afterbody configuration B_2 , the wave-drag reduction due to favorable interference was somewhat less, being about 55 percent. When considering the fact that the model design was somewhat arbitrary, the percentage was fairly high for the concave-afterbody configuration. Possibly part of the drag reduction may have resulted from a change in the boundary-layer conditions on the afterbody, as may be noted in the schlieren photographs of figure 2. In any case, however, the main point of interest appears to be the drag increment for the ring wing and struts; this increment for W_1B_1 is about 84 percent of the total drag. This large wing-drag increment results in such a high total configuration drag that even if zero wave drag were obtained on the body, it appears that the full-ring-wing configuration of these tests would offer no drag advantage over a conventional wing-body configuration. As noted previously, however, the model design was somewhat arbitrary and it would be expected that a more refined design would result in a reduction in the incremental drag associated with the wing and struts.

A comparison of the three ring-wing configurations on the parabolic afterbody B_2 is shown in figure 7. As might be expected, the half-ring-wing configuration W_3B_2 had the lowest minimum drag (0.35) and the highest maximum lift-drag ratio (4.9) of the three configurations. This result is in agreement with the results shown in figure 6, which indicate that the best means for obtaining performance improvement would be in the reduction of wing and strut drag.

It is also interesting to note in figure 7 that the lift-curve slope for the half-ring wing and body combination was different from this slope for the other two wings and that at zero angle of attack, this combination produced a lift coefficient of 0.6 with a corresponding lift-drag ratio of 1.6. The favorable lift increment was apparently produced by the reflection of the forebody positive pressure field on the wing inner surface. In considering other half-ring-wing designs,

L
1
7
3
9

it would be of interest to consider the possibility of further exploitation of the forebody pressure field as a means of producing favorable lift and lift-drag ratios at low angles of attack.

Langley Research Center,
National Aeronautics and Space Administration,
Langley Air Force Base, Va., December 7, 1961.

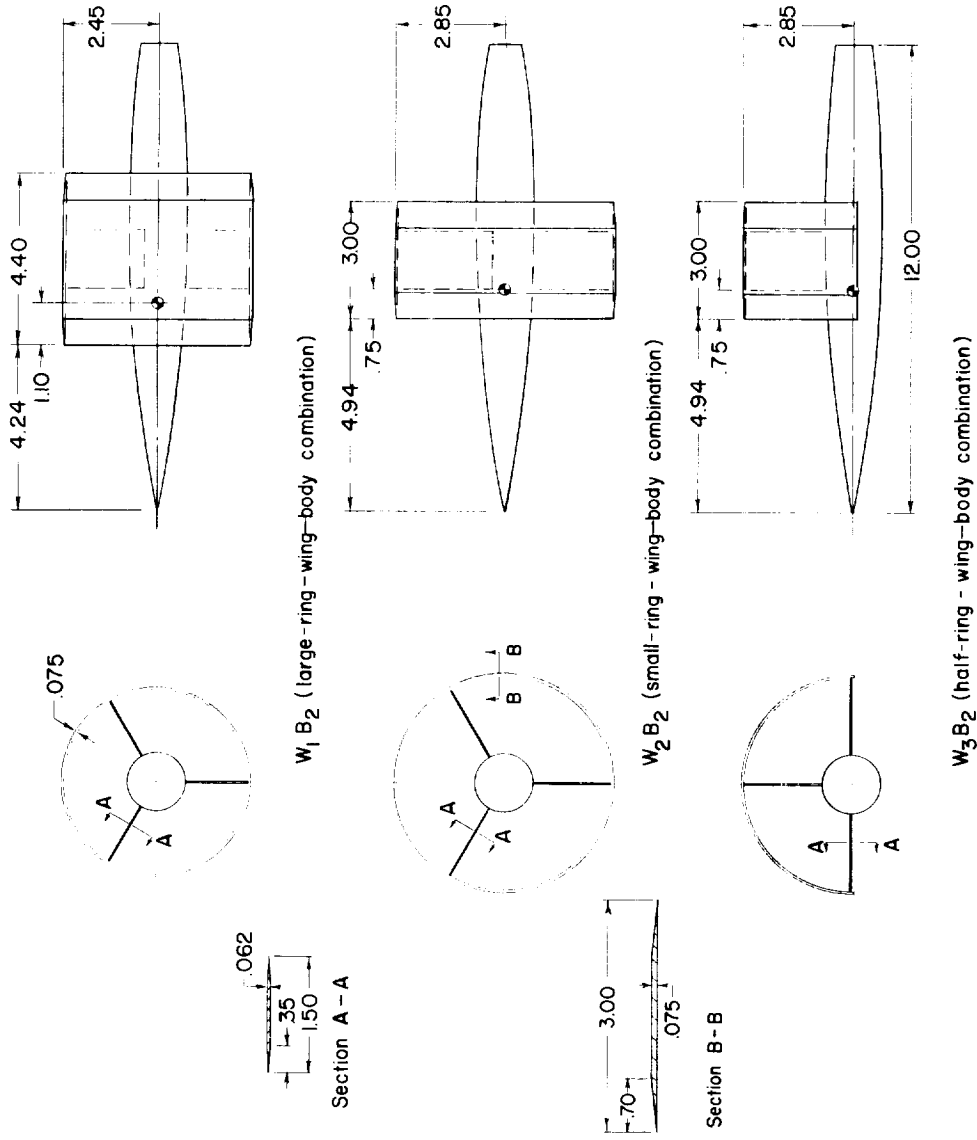
REFERENCES

1. Johnson, Roger P.: Aerodynamic Characteristics and Geometric Properties of Half- and Complete-Ring-Body Configurations for Supersonic Design Mach Number. U.S. Air Force Project RAND Res. Memo. RM-2208 (ASTIA Doc. No. AD 156016), The RAND Corp., July 9, 1958.
2. Johnson, Roger P.: Theoretical Development for Lifting Ring-Body Configurations. U.S. Air Force Project RAND Res. Memo. RM-2260 (ASTIA Doc. No. AD 207751), The RAND Corp., Sept. 9, 1958.
3. Johnson, Roger P.: Verification of Ring-Wing Theory. U.S. Air Force Project RAND Briefing B-224 (Contract No. AF 49(638)-700), The RAND Corp., Jan. 4, 1961.
4. Visich, Marian, Jr., and Martellucci, Anthony: Theoretical and Experimental Analysis of a Cowling as a Means of Drag Reduction for an Axisymmetric Center Body. PIBAL Rep. No. 451 (Contract No. AF 49(638)-217), Polytechnic Inst. Brooklyn, Aug. 1958.
5. Browand, Frederick Kent: The Design and Test of a Zero-Wave-Drag Ring-Wing Configuration. U.S. Air Force Project RAND Res. Memo. RM-2638 (Contract No. AF 49(638)-700), The RAND Corp., June 15, 1960.
6. Broglio, Luigi: Theoretical and Experimental Analysis of Cowling Configurations for the Reduction of the Drag on a Body of Revolution With Large Cone Angle. SIARgraph No. 7 (Contract No. AF - 61 (514) - 816), Scuola di Ingegneria Aeronautica, Universita di Roma, June 1956.
7. Van Driest, E. R.: Turbulent Boundary Layer in Compressible Fluids. Jour. Aero. Sci., vol. 18, no. 3, Mar. 1951, pp. 145-160, 216.

TABLE I. - BODY COORDINATES

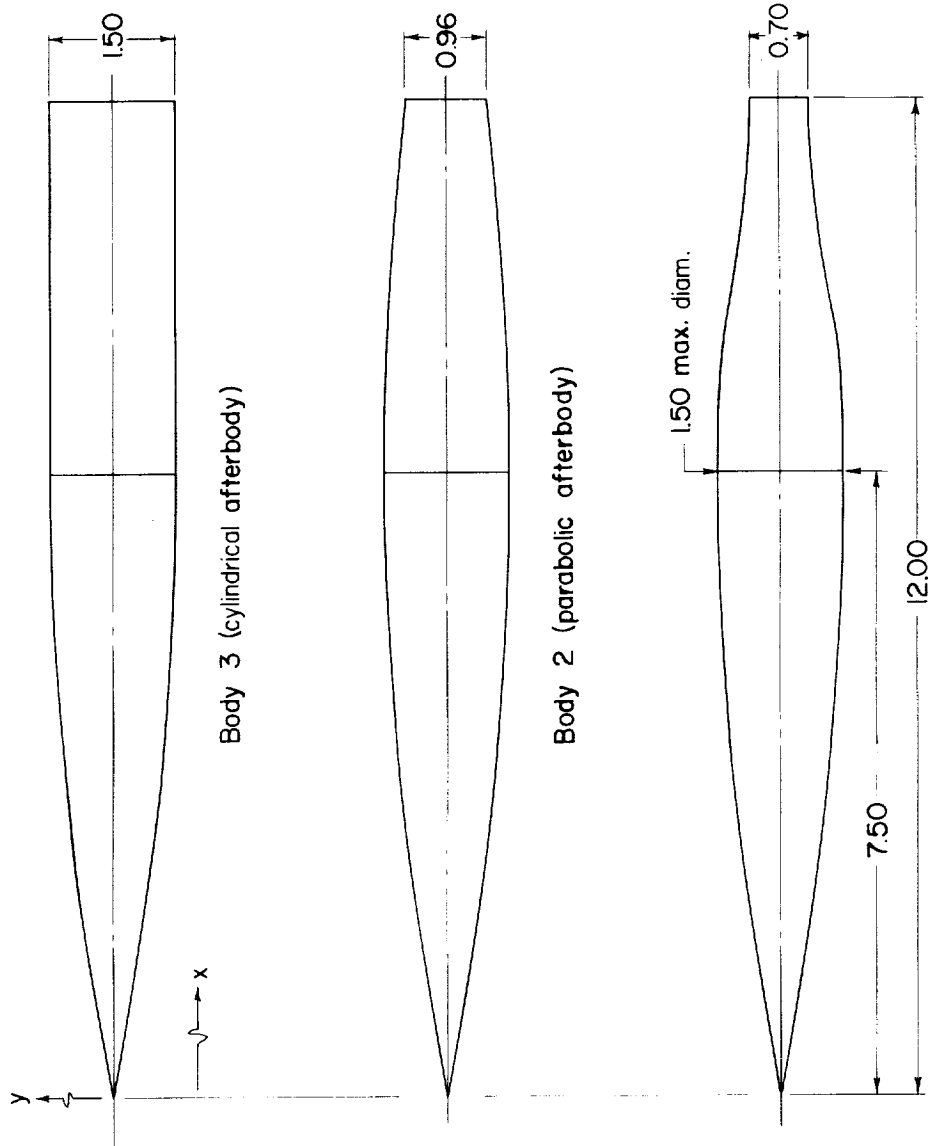
Body section	Coordinates	
	x, in.	y, in.
Nose, B_1 , B_2 , and B_3	0	0
	.375	.073
	.750	.143
	1.125	.208
	1.500	.270
	3.000	.480
	4.500	.630
	6.000	.720
	7.500	.750
Concave afterbody, B_1	7.500	0.750
	8.500	.735
	9.000	.694
	9.500	.620
	10.000	.536
	11.000	.410
	12.000	.350
Parabolic afterbody, B_2	7.500	0.750
	8.500	.735
	9.000	.720
	10.500	.630
	12.000	.480
Cylindrical afterbody, B_3	7.500	0.750
	10.000	.750
	12.000	.750

L
1
7
3
9



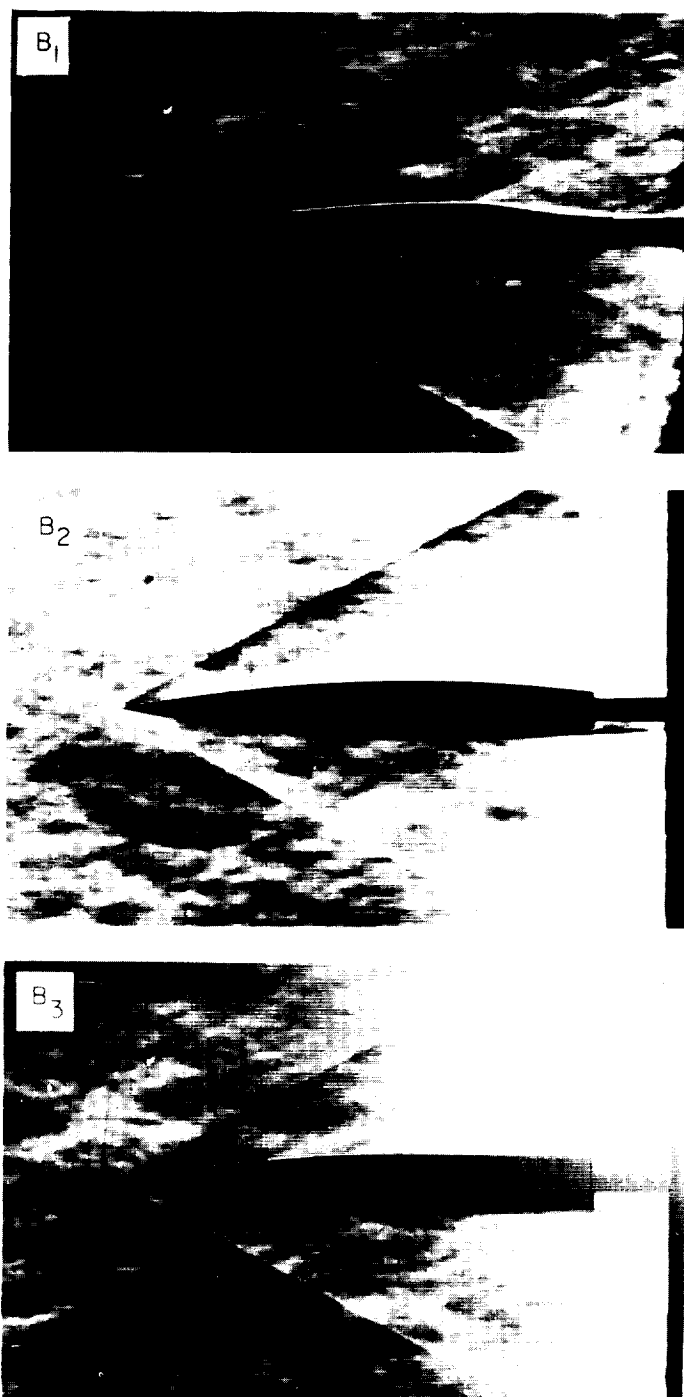
(a) Ring-wing configurations with parabolic body.

Figure 1.- Details of models. All dimensions in inches unless otherwise noted.



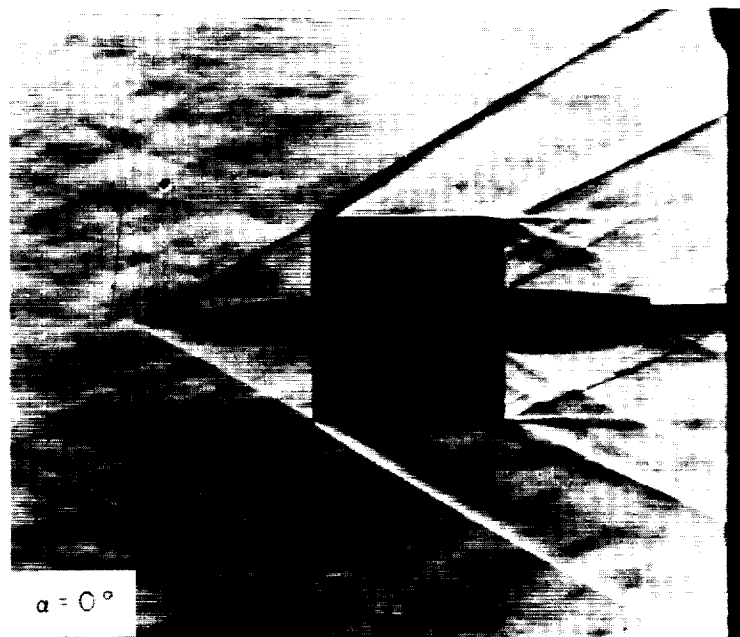
(b) Body shapes.

Figure 1.- Concluded.



(a) Isolated body configurations. $\alpha = 0^\circ$. L-61-8408

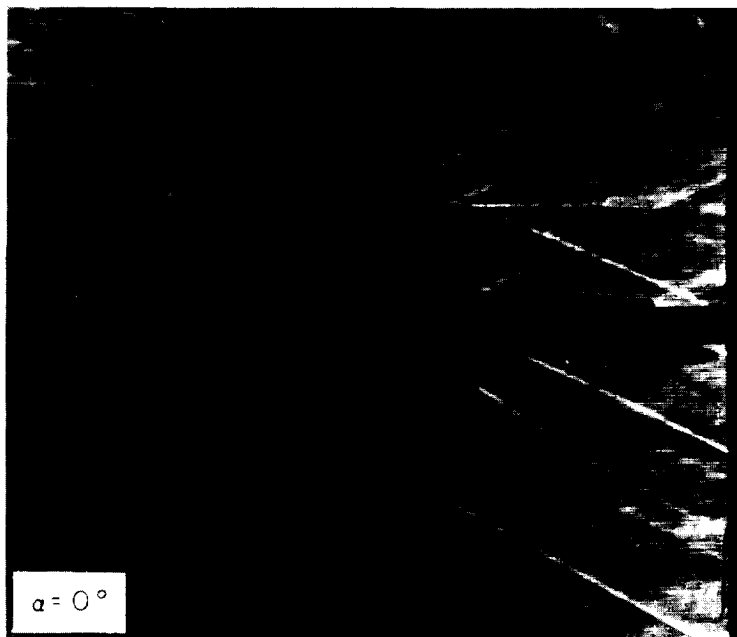
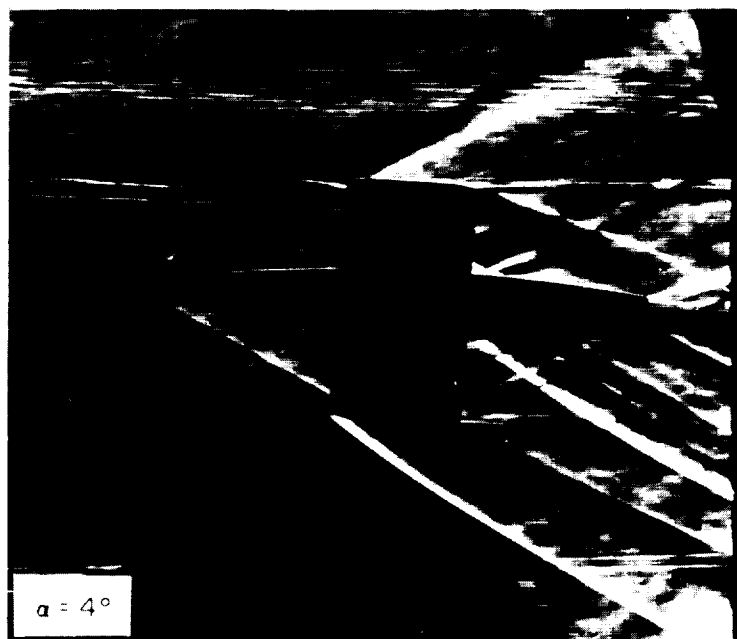
Figure 2.- Schlieren photographs of models. $M = 2.2$.



(b) Large ring wing with parabolic afterbody, W_1B_2 . L-61-8409

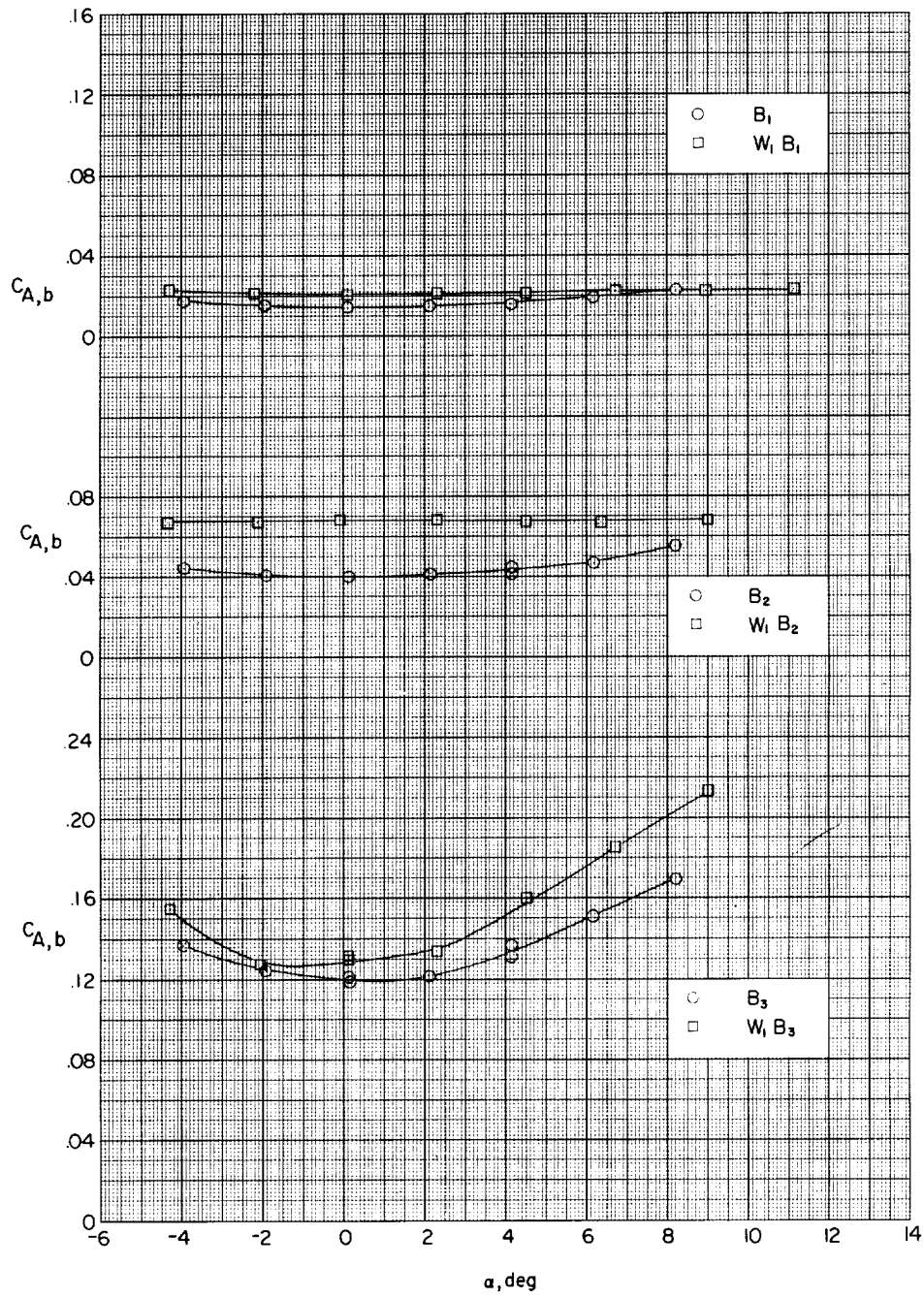
Figure 2.- Continued.

L-1739



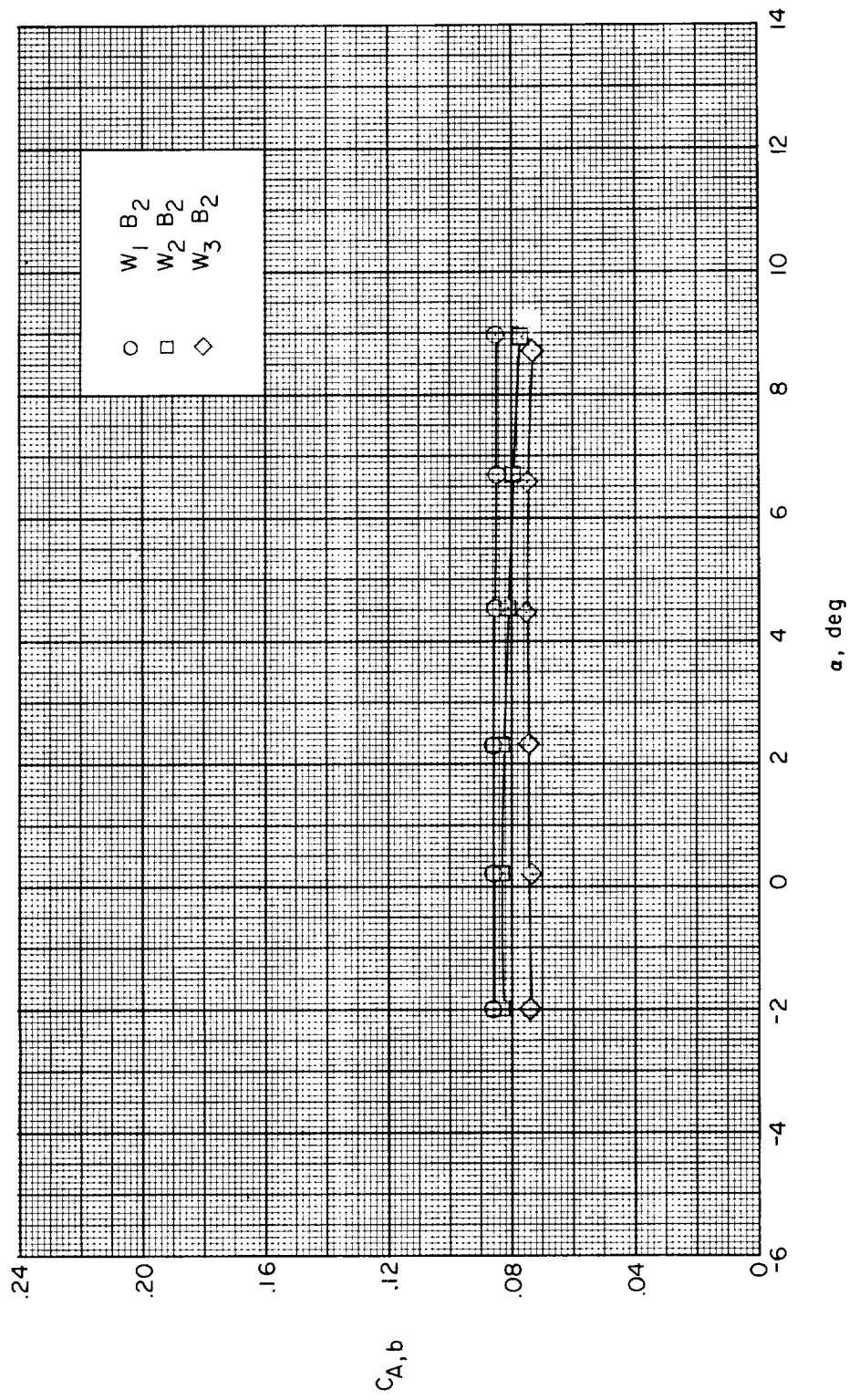
(c) Small ring wing with parabolic afterbody, W_2B_2 . L-61-8410

Figure 2.- Concluded.



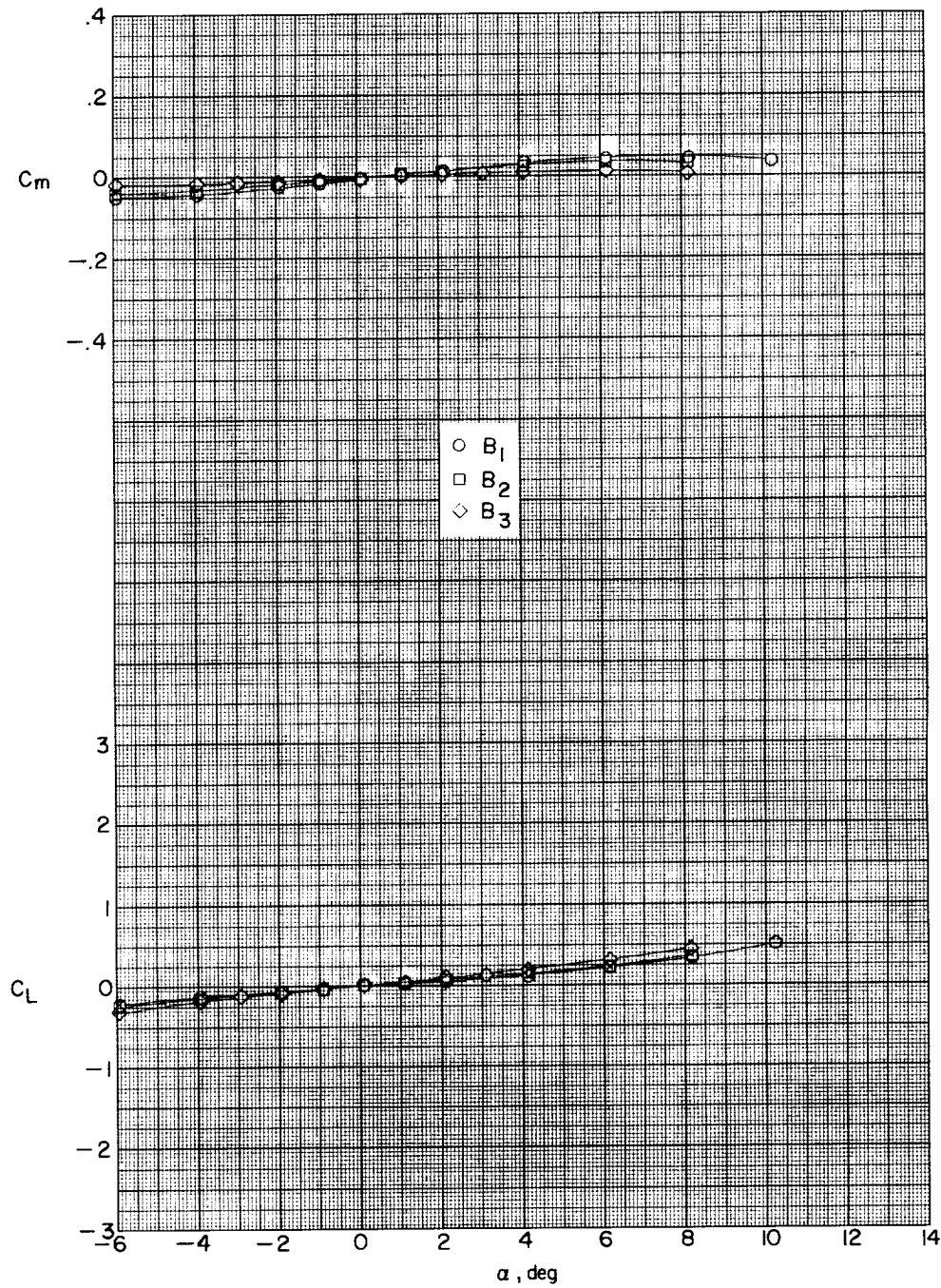
(a) Transition on.

Figure 3.- Variation of body-base axial-force coefficient with angle of attack.



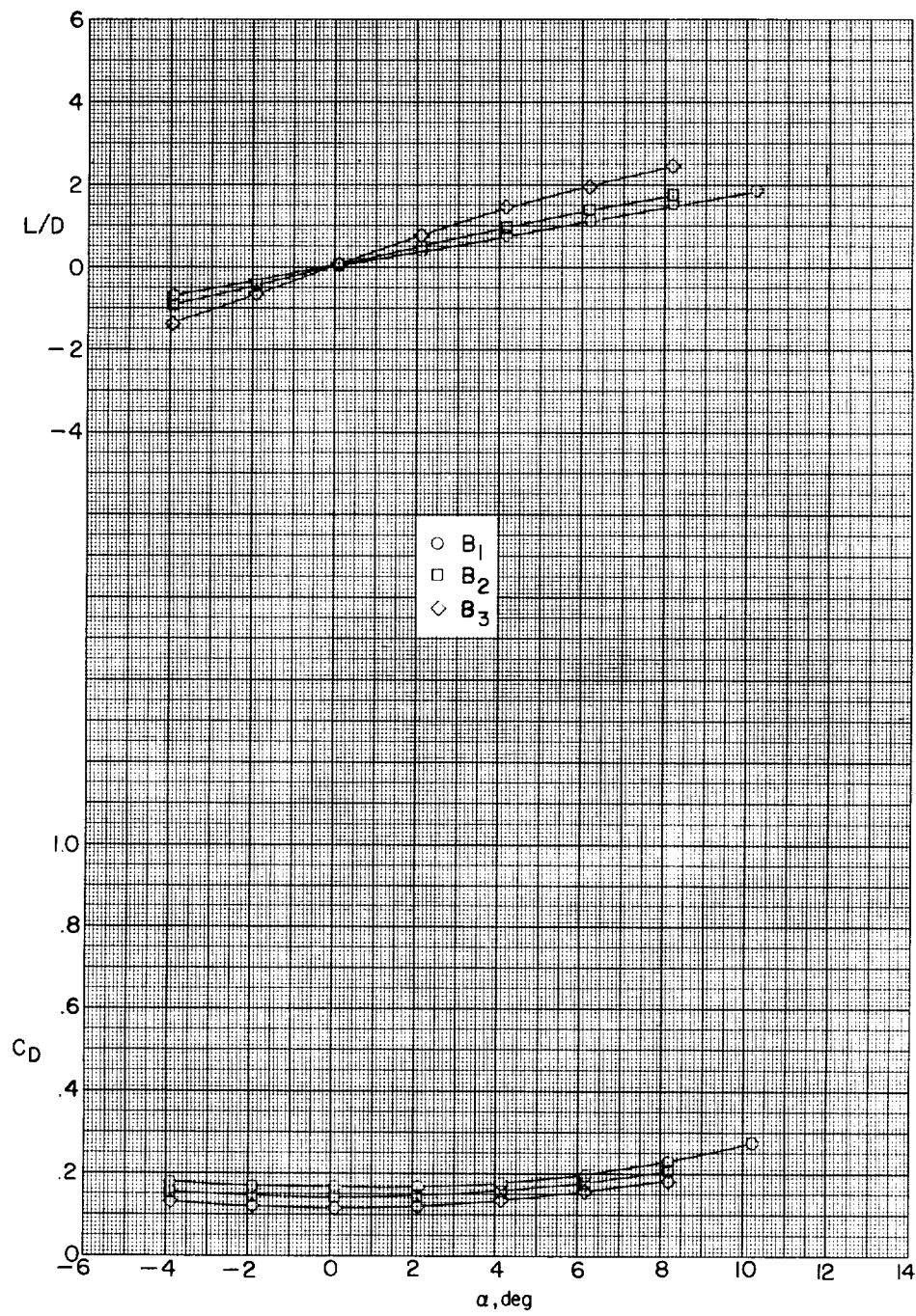
(b) Transition off.

Figure 3.- Concluded.



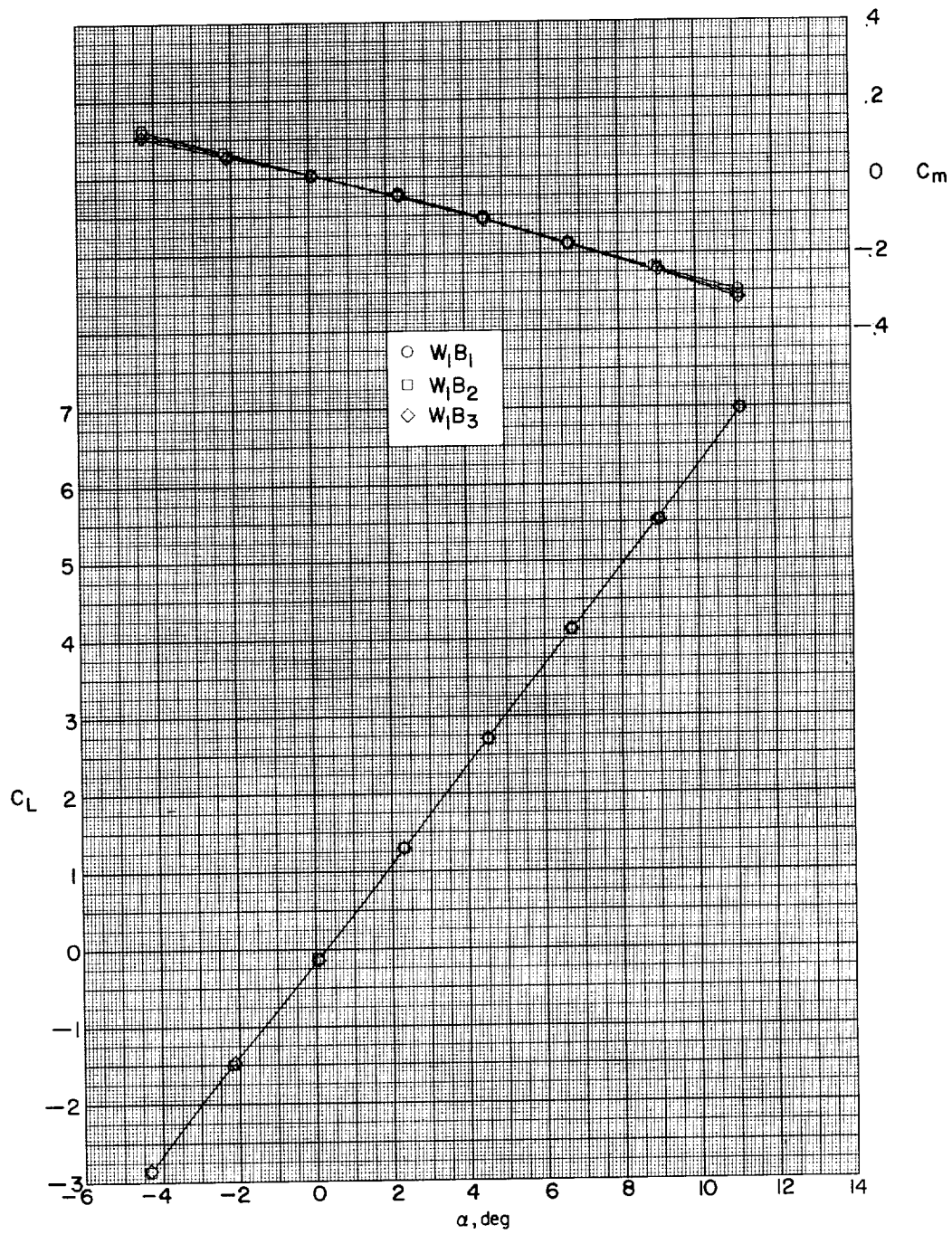
(a) Variation of C_m and C_L with α .

Figure 4.- Aerodynamic characteristics in pitch for isolated bodies.



(b) Variation of L/D and C_D with α .

Figure 4.- Concluded.



(a) Variation of C_m and C_L with α .

Figure 5.- Aerodynamic characteristics in pitch for large ring wing in combination with three afterbodies.

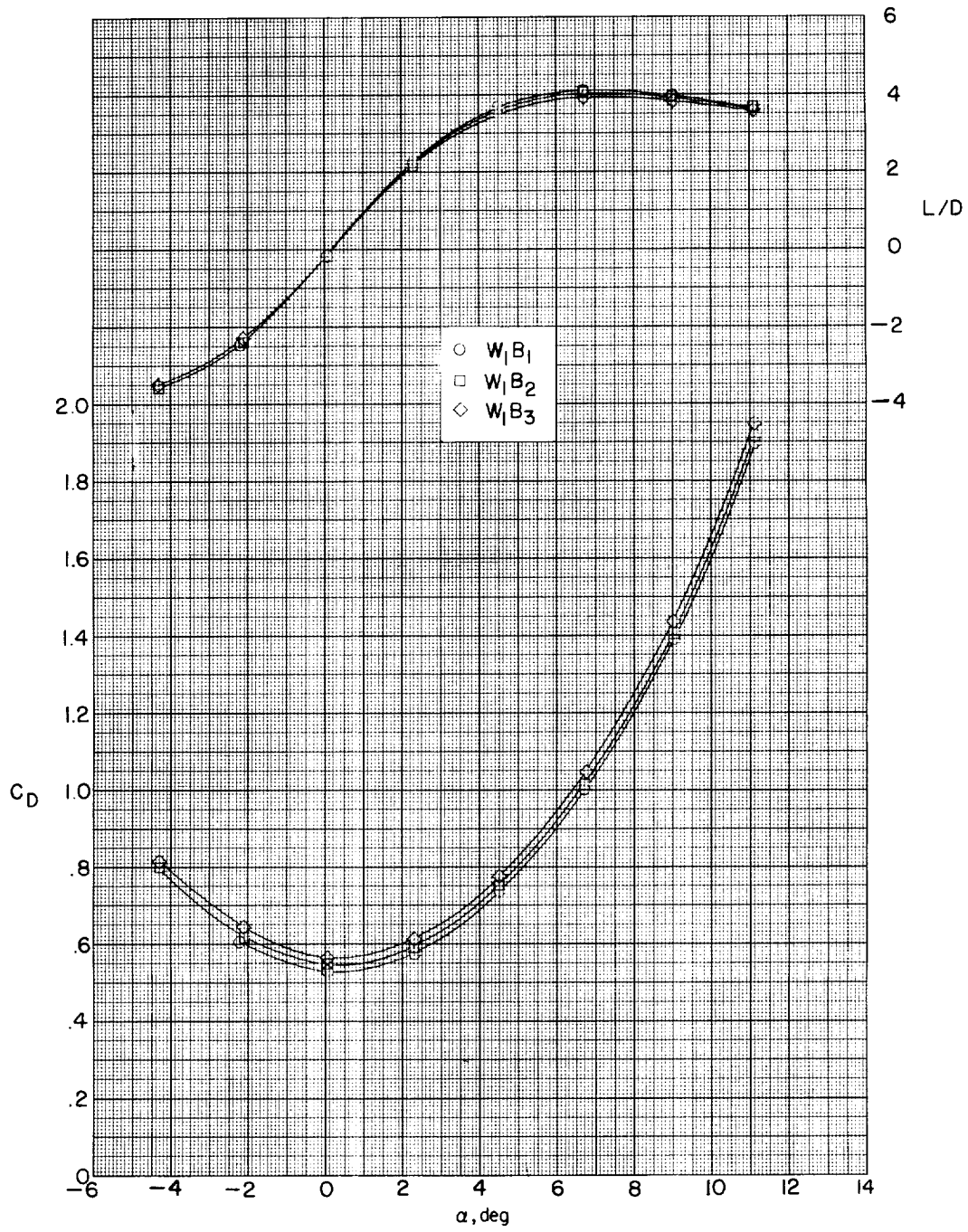
(b) Variation of L/D and C_D with α .

Figure 5.- Concluded.

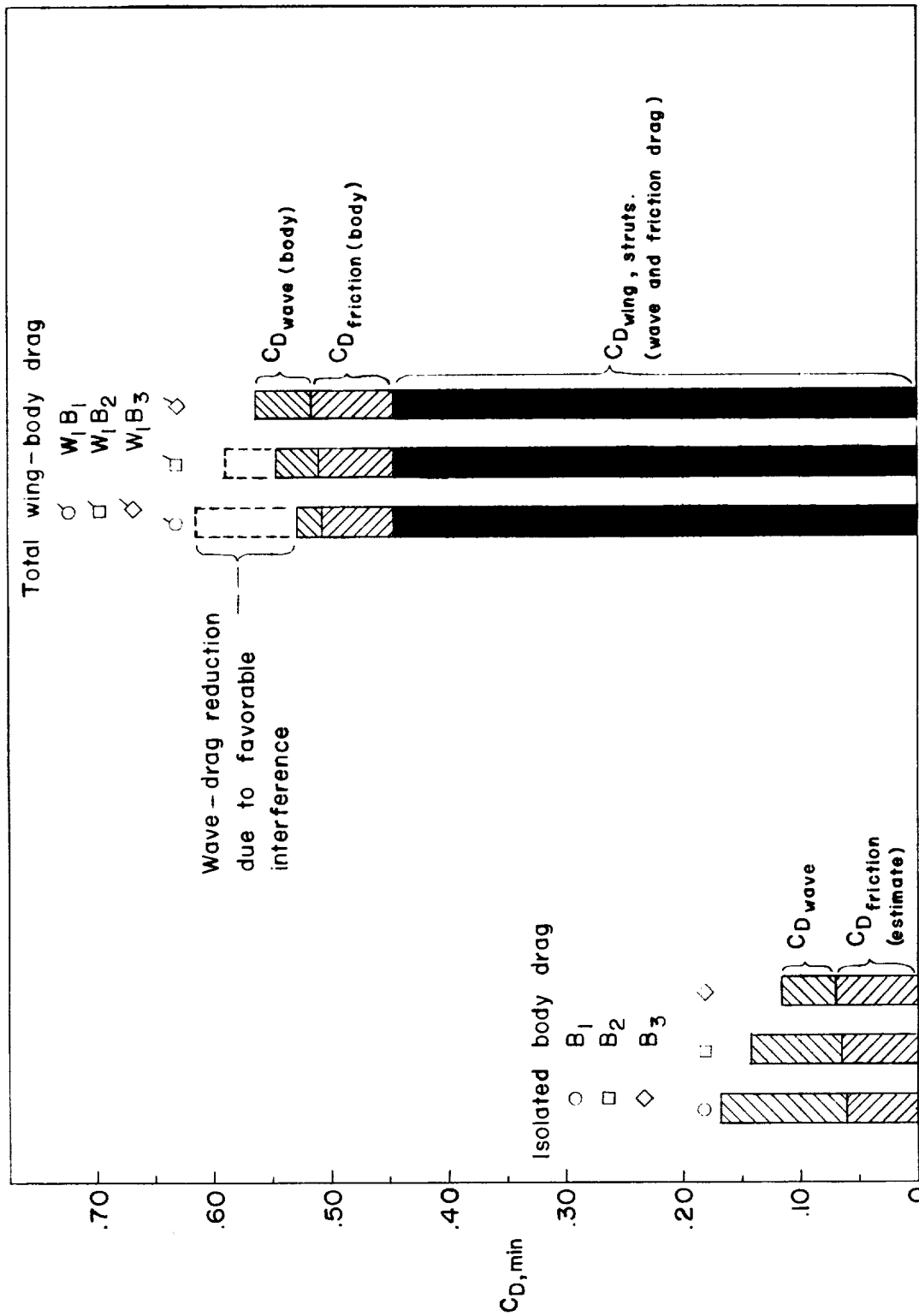
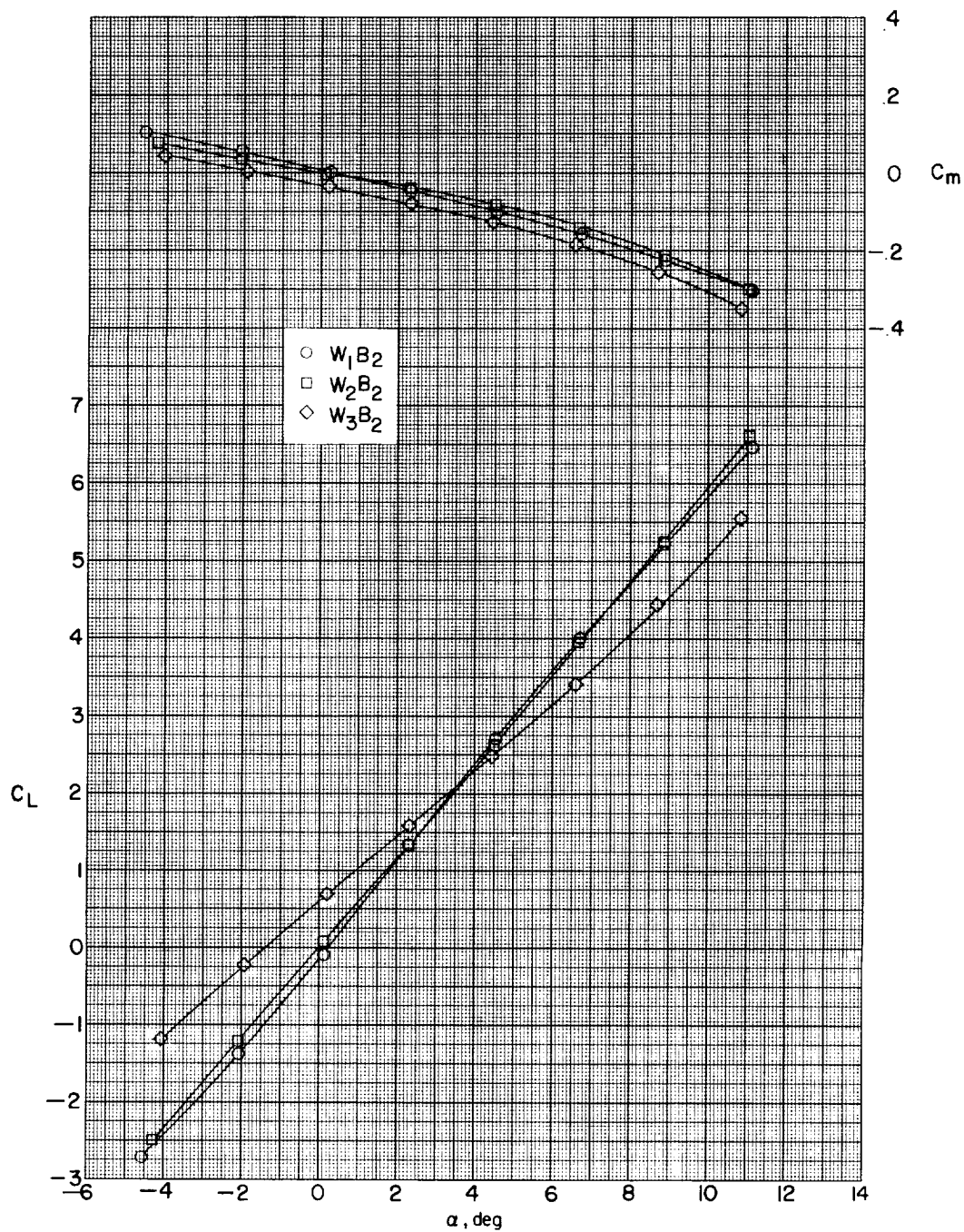
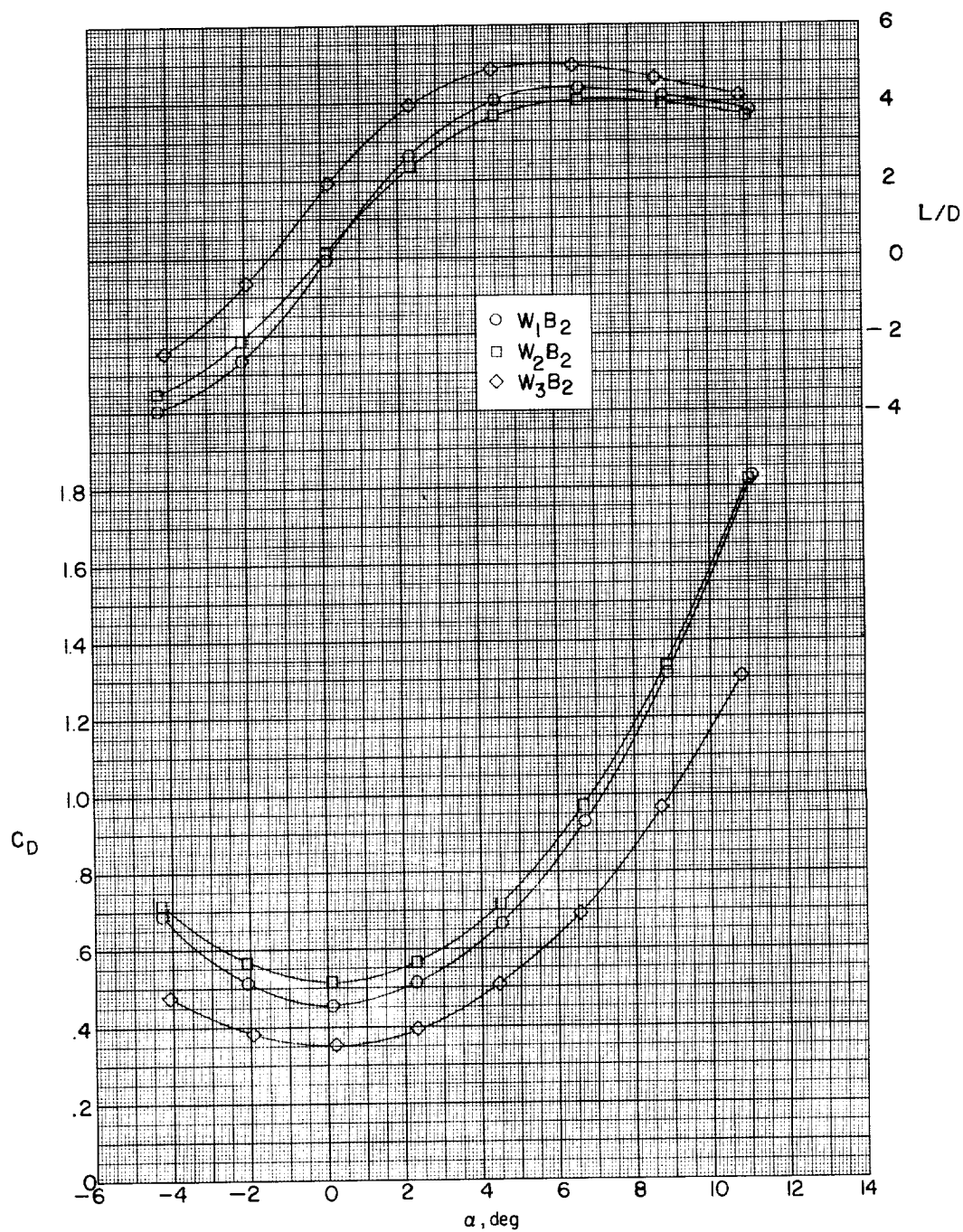


Figure 6.- Drag breakdown for isolated bodies and for large ring wing and body combinations at $\alpha = 0^\circ$.



(a) Variation of C_m and C_L with α .

Figure 7.- Aerodynamic characteristics in pitch for three ring-wing configurations with parabolic afterbody, B_2 (transition strips off).



(b) Variation of L/D and C_D with α .

Figure 7.- Concluded.